Effect of water content on resilient modulus and damping ratio of fine/coarse soil mixtures with varying coarse grain contents

Yu Su, Yu-Jun Cui, Jean-Claude Dupla, Jean Canou

Effect of water content on resilient modulus and damping ratio of fine/coarse soil mixtures with varying coarse grain contents

Yu Su, Yu-Jun Cui, Jean-Claude Dupla, Jean Canou

Laboratoire Navier/CERMES, Ecole des Ponts ParisTech (ENPC), France

Corresponding author

Yu SU

Ecole des Ponts ParisTech, Laboratoire Navier/CERMES, 6 – 8 av. Blaise Pascal, Cité Descartes, Champs-sur-Marne, 77455 Marne – la – Vallée cedex 2, France

E-mail address: yu.su@enpc.fr

Abstract

For the French ancient rail track, owing to the effect of traffic loadings, an interlayer was naturally created due to the interpenetration of ballast grains and subgrade fine soil. Under the effect of rainfall/evaporation, the water content of interlayer soil can vary, affecting its dynamic properties such as resilient modulus and damping ratio. In order to investigate the effect of water content on the resilient modulus and the damping ratio of interlayer soil, a series of cyclic triaxial tests were carried out, following a multi-step loading procedure with various deviator stress amplitudes of 10, 30, 50, 100 and 200 kPa. Two target fines water contents (17.6% and 10.6%) and five coarse grain contents (0%, 10%, 20%, 35% and 45%) were considered. Results showed that under a given coarse grain content, an increase of water content led to a decrease of resilient modulus owing to the decrease of suction while an increase of damping ratio owing to the increase of soil viscosity. Through the variations of resilient modulus and damping ratio with coarse grain content, a characteristic coarse grain content was identified, defining two distinct soil fabrics: a fine soil dominated fabric when the coarse grain content was smaller than the characteristic value, and a coarse grain dominated fabric when the coarse grain content was larger than the characteristic value. Moreover, a constant characteristic coarse grain content was obtained at a given water content: 25.5% at 17.6% water content and 32.0% at 10.6% water content. The increase of characteristic coarse grain content with the decrease of water content could be explained by the swelling-shrinkage of fine soil: with a decrease of water content, the shrinkage of fine soil led to an increase of the volume of macro-pores. More coarse grains were thus needed to constitute the global skeleton, giving rise to an increase of the characteristic coarse grain content. In addition,

comparison of the values of characteristic coarse grain content obtained from cyclic tests with those from monotonic tests showed that at a given water content, cyclic loading led to a slightly larger value than monotonic loading, evidencing the more significant effect of cyclic loading on soil fabric.

Keywords: interlayer soil; cyclic triaxial test; water content; coarse grain content; resilient modulus; damping ratio

48 INTRODUCTION

49 In France, new rail tracks were constructed with a sub-ballast layer which separated the ballast
50 layer from subgrade soil, while ancient tracks were constructed by putting ballast directly on
51 subgrade soil without separation layer. Owing to the effect of train circulation, an interlayer
52 was created in the ancient rail tracks by the interpenetration of ballast grains and subgrade fine
53 soil. Since the interlayer was kept in railway substructure during the national renewal program
54 thanks to its expected favorable mechanical behaviour (Cui et al. 2013), it appears necessary
55 to evaluate its hydro-mechanical behavior, in particular its dynamic properties under traffic
56 loadings.

57 In-situ investigation showed a decrease of ballast grain content over depth (Trinh 2011).
58 Wang et al. (2017, 2018a, 2018b) conducted a series of tests to clarify the effect of coarse
59 grain content f_v (ratio of coarse grains volume to total volume) on the static and dynamic
60 behaviors of interlayer soil under constant water content condition. They identified a
61 characteristic coarse grain content $f_{v\text{-}cha}$, which separated two soil fabrics: one characterized by
62 a fine matrix with dispersed coarse grains and another by a coarse grain skeleton with fines
63 contained in large pores among coarse grains or at the grain/grain contacts. Under rainfall and
64 evaporation, the water content of interlayer soil varies in the field. As a result, the dynamic
65 properties of interlayer soil can change, greatly affecting the mechanical behavior of track
66 bed. Thus, in order to ensure the serviceability of the rail track, the effect of water content on
67 the dynamic properties of interlayer soil should be investigated in depth.

68 The dynamic properties of soils are generally characterized by the resilient modulus and
69 the damping ratio. They are often determined based on the hysteresis loops obtained from

cyclic triaxial tests (Stewart 1982; Selig and Waters 1994; Menq 2003). Lin et al. (2000) investigated the dynamic behavior of a gravelly cobble deposit mixed with fine soil by cyclic triaxial tests. Their results showed that the gravel content greatly affected the nonlinear shear modulus-shear strain and damping ratio-shear strain relations. Tennakoon and Indraratna (2014) studied the dynamic characteristics of fouled ballast by performing a series of large-scale cyclic triaxial tests, and concluded that increasing the fouling magnitude resulted in a decrease of resilient modulus. Wang et al. (2017) and Cui (2018) studied the effect of coarse grain content f_v on the dynamic response of interlayer soil. The results indicated that an increase of coarse grain content f_v gave rise to an increase of resilient modulus and a decrease of damping ratio. Moreover, a characteristic coarse grain content $f_{v\text{-}cha}$ was identified, dividing the soil fabrics into two zones - a fine matrix zone and a coarse grain skeleton zone. Mousa et al. (2020) investigated the effect of proportion of reclaimed asphalt pavement on the resilient modulus behavior of unbound granular materials, and indicated that the addition of reclaimed asphalt pavement tended to increase the resilient modulus of mixtures. The effect of water content was also addressed in some studies. Lamas-Lopez (2016) investigated the effect of water content on the resilient modulus and the damping ratio of the upper part interlayer soil, and reported that an increase of water content resulted in a decrease of resilient modulus and an increase of damping ratio. Zhalehjoo et al. (2018) studied the resilient deformation of unbound granular materials by repeated load triaxial tests, and reported that an increase of water content induced a decrease of resilient modulus. Khasawneh and Al-jamal (2019) analysed a large quantity of data on the resilient modulus of fine-grained soils, and found that the change of water content affected the resilient modulus more significantly than the change

of fine soil content. Jibon et al. (2020) investigated the resilient modulus of subgrade soil by cyclic triaxial tests, and found that the variation of water content significantly affected the resilient modulus of plastic soils, but slightly affected the resilient modulus of non-plastic soil. Duong et al. (2016) investigated the effects of water content and fine soil content on the resilient modulus of the upper part interlayer soil (corresponding to the case of coarse grain skeleton) by large-scale triaxial tests, and found that an increase of water content led to a decrease of resilient modulus. The effect of fine content was found to be strongly related to the water content/degree of saturation. At saturated sate, the higher the fine content the smaller the resilient modulus, while at unsaturated state, the higher the fine content the larger the resilient modulus due to the contribution of suction developed in fine soil.

It is worth noting that a constant dry density ρ_d of soil mixtures was controlled in the study of Duong et al. (2016). Thereby, the suction in soil mixtures changed with changes of coarse grain content f_v, because the dry density of fines changed with f_v. In that case, the dynamic properties identified were the results under the combined effect of suction and f_v. In other words, the effects of suction (or water content) and f_v could not be appreciated separately. In addition, previous studies did not pay attention to the effect of water content on the characteristic coarse grain content $f_{v\text{-}cha}$ under cyclic loadings.

This study aims at investigating the effect of water content on the dynamic properties of the whole interlayer soil with varying coarse grain contents f_v (with thus both the fine matrix fabric and coarse grain skeleton fabric). Note that the fine dry density $\rho_{d\text{-}f}$ remained constant for all samples, allowing a constant suction of soil mixtures with varying f_v values. Cyclic triaxial tests were performed for this purpose. A multi-step loading procedure with various

loading amplitudes (10, 30, 50, 100 and 200 kPa) was adopted. Two water contents (17.6% and 10.6%) and five coarse grain contents (0%, 10%, 20%, 35%, and 45%) were considered. The obtained results allowed the resilient modulus and the damping ratio to be determined, and their variations with coarse grain content and water content to be further analysed.

MATERIALS AND METHODS

Fine soil and coarse grains

Considering the extreme difficulty of extracting intact interlayer soil from the field for large quantity and limited variability, reconstituted soil was fabricated instead in the laboratory using both fine-grained and coarse-grained soils. The fine soil part was fabricated using nine different commercial soils (Table 1), keeping the grain size distribution similar to that from 'Senissiat site' (Trinh 2011), as shown in Fig. 1. The liquid limit and the plasticity index of the reconstituted fine soil were 32% and 20%, respectively. Following ASTM D698-12, the standard proctor compaction curve of reconstituted fine soil was determined (Fig. 2), defining an optimum water content $w_{opt\text{-}f}$ = 13.7% and a maximum dry density $\rho_{dmax\text{-}f}$ = 1.82 Mg/m^3.

For the coarse grains part, following the similitude method applied by Wang et al. (2018a) and Qi et al. (2019) and verified later by Qi et al. (2020), micro-ballast was adopted to replace the real ballast (Fig.1). Parameter f_v was adopted to represent the amount of micro-ballast in the fine/coarse soil mixtures. Under a given f_v value, the dry mass of coarse grains and dry mass of fine soil could be determined (see details in Wang et al. (2018a)).

In order to prepare a sample at a target coarse grain content f_v and a target water content of fine soil w_f, the fine soil was prepared at the optimum water content $w_{opt\text{-}f}$ = 13.7%, then preserved in a container for 24 h allowing moisture homogenization. The fine soil was then mixed thoroughly with micro-ballast at the pre-determined mass to reach the target f_v value. After that, the soil mixture was dynamically compacted in three layers, with the equivalent amounts of fine soil and coarse grains for each layer, to finally attain a diameter of 100 mm and a height of 200 mm. It is worth noting that the fine soil in all samples was fixed at a dry unit mass $\rho_{dmax\text{-}f}$ = 1.82 Mg/m^3 (Table 2). Thus, more compaction energy was required for the sample at higher f_v value, resulting in a higher dry unit mass ρ_d as shown in Table 2.

After obtaining the target f_v value, either a wetting or a drying process was applied to attain a target w_f value: w_1 = 17.6% (S_r = 100%) on the wet side of optimum or w_2 = 10.6% (S_r = 60%) on the dry side of optimum (Fig.2). For this purpose, a method proposed by Su et al. (2020a) was adopted: in the case of drying, the sample was each time exposed to the air in the laboratory for 1 h and then covered with plastic film for at least 7 h equilibration. In the case of wetting, 10 g water was each time sprayed on the sample before wrapping it with plastic film for at least 7 h equilibration. Fig. 3 indicates that either swelling or shrinkage of samples at different f_v values occurred, upon wetting from $w_{opt\text{-}f}$ = 13.7% to w_1 = 17.6% or drying from $w_{opt\text{-}f}$ = 13.7% to w_2 = 10.6%. It appears that the swelling-shrinkage of sample decreased with the increase of f_v value, indicating the sensitivity of fine soil to water content change. The measured ρ_d of samples after wetting or drying to the target w_f value are presented in Table 2.

Cyclic triaxial tests

155 The cyclic triaxial apparatus used by Wang et al. (2017) was adopted in this study, hosting a
156 sample of 100 mm diameter and 200 mm height. A 50 kN hydraulic actuator was adopted,
157 enabling either a displacement or force controlled mode in monotonic and cyclic triaxial tests.
158 For the cyclic loading, different signal shapes, amplitudes, frequencies and large number of
159 cycles (up to several millions) could be applied. A linear variable displacement transducer
160 (LVDT) was used for the measurement of axial displacement, and a force sensor installed at
161 the bottom allowed the monitoring of axial force.

162 Cyclic triaxial tests were performed on the samples at two water contents (w_1 = 17.6%
163 and w_2 = 10.6%) and five different f_v values (0%, 10%, 20%, 35% and 45%) with the drainage
164 valve open. A confining pressure σ_3 = 30 kPa was applied in all tests, which corresponded to
165 the average horizontal stress estimated in the field condition by considering the train loading,
166 the depth of interlayer and the Poisson's ratio (Duong et al. 2016). For the samples at w_1 =
167 17.6% (S_r = 100%), an overnight consolidation under σ_3 = 30 kPa was adopted prior to the
168 cyclic loading, because in that case pore water pressure could be generated. By contrast, for
169 samples at w_2 = 10.6% (S_r = 60%), after application of σ_3 = 30 kPa, the cyclic loading was
170 performed directly, for only air was expected to be expelled. Fig. 4 depicts the various sine-
171 shaped signals applied at a frequency of 1.78 Hz corresponding to that excited between two
172 bogies at a train speed of 50 km/h.

173 A series of cyclic loadings with various loading amplitudes Δq = 10, 15, 20, 25 and 30
174 kPa were applied, with a number of loading cycles N = 90000 for each Δq value. Note that Δq
175 was defined as the difference between the maximum deviator stress q_{max} and the minimum
176 deviator stress q_{min}. After that, the multi-step loading procedure proposed by Gidel et al. (2001)

and applied later by Duong et al. (2016) and Wang et al. (2017) was adopted, as shown in Fig. 5 with Δq plotted against N. The values of Δq at 10, 30, 50, 100 and 200 kPa were applied and each with N = 100 cycles, as in Lamas-Lopez (2016) and Wang et al. (2017). These Δq values were selected by accounting for the train wheel load and the depth of interlayer soil from 250 mm to 600 mm. Considering the wheel load of 16-22 tons per axle in France and 30 tons per axle of heavier train in other countries (Alias 1984), the corresponding range of vertical stress was estimated at 40 - 90 kPa and 120 - 140 kPa (Duong et al. 2013), respectively. A maximum value of Δq = 200 kPa was adopted to consider the maximum vertical stress distributed on the top of railway substructure. Note that the application of Δq equal to 10 and 30 kPa was to ensure the continuity of a multi-step loading stresses Δq. During the tests, the axial force and axial displacement were monitored.

EXPERIMENTAL RESULTS

Fig. 6 depicts typical hysteresis loops for various deviator stress amplitudes Δq at f_v = 0% and two target water contents. It can be observed that at a given water content, the size of hysteresis loop increased with the increase of Δq. When $\Delta q \leq$ 30 kPa, the hysteresis loops were small because of the large number of loading cycles applied under this stress level to approach an in-situ soil state, prior to starting the multi-step loading procedure shown in Fig. 5. By contrast, when Δq increased to a larger value, especially at 100 kPa for w_1 =17.6% and 200 kPa for w_2 = 10.6%, a larger unclosed hysteresis loop occurred, with the axial strain consisting of two parts: permanent strain ε_1^p and elastic strain ε_1^r. Note that at w_1 =17.6%, the used LVDT reached its measurement capacity around 70 mm by the end of loading under Δq

199 = 100 kPa. Thus, the tests at w_1 =17.6% ended at N = 1400 (Fig. 5). In addition, a decrease of
200 water content from w_1 =17.6% to w_2 = 10.6% led to a decrease of the size of hysteresis loops,
201 indicating that both permanent strain ε_1^p and elastic strain ε_1^r decreased with the decrease of
202 water content.

203 To further clarify the effect of water content, the variations of ε_1^p and ε_1^r with loading
204 cycles N at f_v = 0% are plotted in Fig. 7 for the two target water contents. At a given water
205 content, the permanent strain ε_1^p and elastic strain ε_1^r increased slowly with Δq until Δq = 100 -
206 200 kPa. Then, a sharp increase was observed for both strains. As shown in Fig. 7, the
207 decrease of water content from w_1 =17.6% (Fig. 7 (a_1) - (b_1)) to w_2 = 10.6% (Fig. 7 (a_2) - (b_2))
208 resulted in a large decrease of both strains.

209 Fig. 8 illustrates the variation of hysteresis loops with N for the first 100 cycles of Δq =
210 100 kPa at f_v = 0% and two target water contents. At w_1 = 17.6%, the size of hysteresis loop
211 became smaller and more stable with the increase of N, which could be explained by the
212 decrease of permanent strain ε_1^p and eventually a purely resilient behavior. The same
213 observation could be made for w_2 = 10.6%. Furthermore, when the water content decreased
214 from w_1 = 17.6% to w_2 = 10.6%, the size of hysteresis loop decreased largely, suggesting that
215 a decrease of water content promoted the resilient behavior.

216 Fig. 9 (a) defines the resilient modulus M_r as the secant slope of hysteresis loop (Seed et
217 al. 1986; Rollins et al.1998; Tennakoon and Indraratna 2014):

218 $$M_r = \frac{\Delta q}{\varepsilon_1^r} \quad (1)$$

219 where Δq is the deviator stress amplitude, ε_1^r is the resilient strain.

220 Fig. 9 (b) defines the damping ratio D_r as the ratio of dissipated energy to the total energy
221 during a given cycle (Seed et al. 1986; Rollins et al.1998; Tennakoon and Indraratna 2014):

222 $$D_r = \frac{E_{loop}}{4\pi E_d} \quad (2)$$

223 where E_{loop} is the area of hysteresis loop, E_d is the area of triangle, which is determined by the
224 maximum deviator stress and the maximum axial strain in one cycle.

225 Fig. 10 depicts the variations of M_r with N under the two target water contents. It appears
226 clearly that a higher water content gave rise to a lower M_r. Moreover, at a lower content w_2 =
227 10.6%, M_r appeared to increase with the increase of Δq; in particular, a sudden increase at the
228 first cycle and a stabilization at the end were identified. The variations of M_r with Δq at a
229 higher water content w_1 = 17.6% were not as clear as that at w_2 = 10.6%: the first increases of
230 Δq up to 50 kPa seemed to decrease M_r; the second increases of Δq up to 100 kPa did not
231 affect M_r and the third increases of Δq also seemed to decrease M_r. Thus, opposite variation
232 trends of M_r with Δq could occur when increasing the water content from 10.6% to 17.6%.
233 The similar phenomenon was reported by Yang et al. (2008) on subgrade soil through suction-
234 controlled cyclic triaxial tests. They found that M_r decreased with the increasing Δq at low
235 matrix suctions ranging from 50 to 150 kPa, while increased with the increasing Δq at a high
236 matrix suction of 450 kPa. Ng et al. (2013) studied the effects of Δq and suction on M_r of
237 subgrade soil by suction-controlled cyclic triaxial tests, and reported that M_r decreased with
238 the increase of Δq at low matrix suctions ranging from 0 to 250 kPa. Moreover, they
239 developed a model describing the variations of M_r with Δq considering the opposite variation
240 trends of M_r with Δq in low and high suctions ranges. Han and Vanapalli (2015) also proposed

241 a model describing the variation of M_r of subgrade soil with suction using the soil-water
242 retention curve. But their model did not take the effect of Δq into account.

243 To further analyze the effect of water content on resilient modulus M_r, the values of M_r at
244 the first cycles (start-stages) and last cycles (end-stages) of Δq = 50, 100 and 200 kPa are
245 chosen for comparison in Fig. 11 for the five different f_v values and two different w_f values.
246 Note that the legend "N201-50kPa" referred to the number of loading cycles N = 201 and the
247 deviator stress amplitude Δq = 50 kPa. Figs. 11 (a_1) - (b_1) show that in the case of w_1 = 17.6%,
248 at the start-stages of Δq = 50 and 100 kPa, M_r increased slowly with f_v at $f_v \leq 20\%$, while a
249 large increase of M_r with f_v occurred at $f_v \geq 35\%$. A bilinear fitting was attempted for such M_r
250 variation. It could be found that at the start-stages of Δq = 50 and 100 kPa, a quite similar
251 characteristic coarse grain content $f_{v\text{-}cha} \approx 25.5\%$ was identified at the intersection points of two
252 fitting lines, indicating that the $f_{v\text{-}cha}$ was independent of stress amplitude Δq. It could be
253 deduced that when $f_v \leq f_{v\text{-}cha,}$ the fine soil dominated the fabric of soil mixtures and the
254 increase of coarse grain content f_v led to a slight increase of M_r. By contrast, when $f_v \geq f_{v\text{-}cha}$,
255 the coarse grains dominated the soil fabric and the increase of f_v led to a significant increase of
256 M_r.

257 When it comes to the end-stages of Δq = 50 and 100 kPa (Figs. 11 (a_2) - (b_2)), the same
258 observation was made in terms of variations of M_r with f_v. Interestingly, while fitting the
259 distinct increasing rates of M_r with f_v at $f_v \leq 20\%$ and $f_v \geq 35\%$, the value of $f_{v\text{-}cha}$ appeared to
260 approach 25.5%, in agreement with the value identified based on the data corresponding to the
261 start-stages of Δq = 50 and 100 kPa.

Figs. 12 (a_1) - (b_1) show the different variations of M_r with f_v at $f_v \leq 20\%$ and $f_v \geq 35\%$ at the start-stages of Δq = 50, 100 and 200 kPa for the case of w_2 = 10.6%. A characteristic coarse grain content $f_{v\text{-}cha}$ was identified around 32.0% for various stress amplitudes Δq. The similar phenomenon could be observed for the end-stages of Δq = 50, 100 and 200 kPa (Figs. 12 (a_2) - (b_2)). Using two lines to fit the increasing trend of M_r with f_v, the value of $f_{v\text{-}cha}$ was found to be 32.0%, in agreement with the value identified using data corresponding to the start-stages of Δq = 50, 100 and 200 kPa.

Fig. 13 depicts the effect of water content on D_r at f_v = 0%. Under a constant water content, D_r increased sharply with Δq at the first loading cycle, and then decreased gradually until a stable state. This can be explained by the evolution of hysteresis loops with N at a given Δq value, as observed in Fig. 8: at a constant w_f value and Δq = 100 kPa, the size of hysteresis loops decreased with N, suggesting less energy loss and giving rise to a smaller D_r value. When the water content decreased from w_1 = 17.6% to w_2 = 10.6%, a significant decrease of D_r was observed, which was also in agreement with the variation of the size of hysteresis loops shown in Figs. 8 (a) - (b).

To further clarify the effect of water content on D_r, the values of D_r at the first cycles (start-stages) and the last cycles (end-stages) of Δq = 50, 100 and 200 kPa were selected for comparison. Figs. 14 (a_1) - (b_1) show two distinct decreasing slopes of D_r with f_v at $f_v \leq 20\%$ and $f_v \geq 35\%$ respectively for the start-stages of Δq = 50 and 100 kPa in the case of w_1 = 17.6%. A characteristic coarse grain content $f_{v\text{-}cha}$ could be also identified, around 25.5% under different Δq values. The same phenomenon was observed in Figs. 14 (a_2) - (b_2) for the end-stages of Δq = 50 and 100 kPa: applying two lines to fit the variation of D_r with f_v at $f_v \leq$

20% and $f_v \geq 35\%$ respectively, a value of $f_{v\text{-}cha}$ was identified, also around 25.5%. Interestingly, this $f_{v\text{-}cha}$ value was in good concordance with the value identified based on M_r data (Fig.11).

Fig. 15 shows the variation of D_r with f_v under various Δq values in the case of w_2 = 10.6%. No matter at the start-stages or end-stages of Δq = 50, 100 and 200 kPa, two different decreasing trends at $f_v \leq 20\%$ and $f_v \geq 35\%$ could be identified, defining a value of $f_{v\text{-}cha}$ close to 32.0%. This value was also in good concordance with that identified with M_r data (Fig. 12).

INTERPRETATION AND DISCUSSION

Based on the variations of M_r and D_r with f_v, a constant $f_{v\text{-}cha}$ value was obtained at a given water content: $f_{v\text{-}cha} \approx 25.5\%$ at w_1 = 17.6% and $f_{v\text{-}cha} \approx 32.0\%$ at w_2 = 10.6%. Note that at $w_{opt\text{-}f}$ = 13.7% a narrow range of $f_{v\text{-}cha}$ from 27.8% to 28.9% was found by Wang et al. (2017), defining an average value of 28.4%. This average value was considered in further analysis. It appears clearly from Table 3 that $f_{v\text{-}cha}$ increased with the decrease of water content.

As reported by Wang et al. (2017) and Qi et al. (2019), the effect of coarse grain content f_v separated the soil fabrics of mixtures into two zones: a zone corresponding to a fine soil supported fabric at $f_v \leq f_{v\text{-}cha}$ and a zone corresponding to a coarse grain supported fabric at $f_v \geq f_{v\text{-}cha}$. According to Su et al. (2020a), two categories of fines existed in the coarse grain skeleton: the first category of dense fines in-between coarse grains and the second category of looser fines situated in the macro-pores surrounded by coarse grains. The former was expected to contribute to the force transmission between coarse grains, as shown by de Frias

Lopez et al. (2016) on fine-coarse granular mixtures through discrete element analysis and Qi et al. (2020) through the dynamic response of track-bed materials in cyclic triaxial tests.

The variation of $f_{v\text{-}cha}$ with water content could be explained by the swelling or shrinkage of fine soil, which contained 30% of clay soils (Speswhite and Bentonite) as shown in Table 1. When the water content decreased, shrinkage of both categories of fines occurred. The shrinkage of dense fines led to a decrease of the volume of macro-pores, whereas the shrinkage of loose fines resulted in an increase of the volume of macro-pores. The variation of the global volume of macro-pores was the result of the competition between the dense and loose fines. Owing to the expected higher density and smaller amount of dense fines, the variation of global volume of macro-pores was expected to be governed mainly by the volume change of loose fines. Thereby, an increase of global volume of macro-pores was expected during the drying process. The similar observation was made by Zhang and Li (2010) on fine/coarse soil mixtures using mercury intrusion porosimetry technique. They found that in the case of coarse grain supported structure, the shrinkage of fines upon drying led to a slight volume change of soil mixtures, but gave rise to a significant increase of volume of macro-pores. With a larger volume of macro-pores, more coarse grains were needed to constitute a global skeleton, giving rise to an increase of $f_{v\text{-}cha}$ value.

Su et al. (2020b) also identified the $f_{v\text{-}cha}$ values at different water contents by performing monotonic triaxial tests: $f_{v\text{-}cha} \approx 25\%$ at $w_1 = 17.6\%$, $f_{v\text{-}cha} \approx 27\%$ at $w_{opt\text{-}f} = 13.7\%$ and $f_{v\text{-}cha} \approx 29\%$ at $w_2 = 10.6\%$. Comparison between these $f_{v\text{-}cha}$ values and those obtained in this study by cyclic triaxial tests showed that for a given water content, a slightly larger $f_{v\text{-}cha}$ value was obtained under cyclic loading. This could be explained by the more efficient effect of cyclic

327 loading on the rearrangement of coarse grains. The similar phenomenon was observed by
328 Duong et al. (2016) on upper part of interlayer soil, who reported that the cyclic loading
329 resulted in a progressive stabilization of particles arrangement. Werkmeister et al. (2004)
330 investigated the volume change behavior of unbound granular materials by cyclic triaxial tests,
331 and found that the cyclic loading induced a denser soil structure and an increase of coarse
332 grain contacts. It could be thus inferred that a relatively larger reduction of macro-pore
333 volume is expected under cyclic loading, increasing the fraction of coarse grains required for
334 constituting a grain skeleton fabric and leading to a larger $f_{v\text{-}cha}$ value.
335

336 CONCLUSIONS

337 To investigate the effect of water content on the dynamic properties of interlayer soil, a series
338 of cyclic triaxial tests were performed, following a multi-step loading procedure with various
339 Δq values. Two target fine water contents w_f (w_1 = 17.6% and w_2 = 10.6%) and five coarse
340 grain contents f_v (0%, 10%, 20%, 35% and 45%) were considered, aiming at investigating the
341 variations of the resilient modulus M_r and the damping ratio D_r with w_f and f_v. In particular,
342 the values of M_r and D_r at the start-stages and end-stages of Δq = 50, 100 and 200 kPa were
343 selected for comparison. The following conclusions were drawn:

344 Under a given f_v value, the increase of water content led to a decrease of M_r due to the
345 contribution of suction while an increase of D_r owing to the increase of soil viscosity.
346 Through the variations of M_r and D_r with $f_{v,}$ a characteristic coarse grain content $f_{v\text{-}cha}$ was
347 identified, defining two distinct soil fabrics: a fine matrix fabric at $f_v \leq f_{v\text{-}cha}$ and a coarse grain
348 skeleton fabric at $f_v \geq f_{v\text{-}cha.}$ Moreover, a constant $f_{v\text{-}cha}$ value was obtained at a given water

content: $f_{v\text{-}cha} \approx 25.5\%$ at $w_1 = 17.6\%$ and $f_{v\text{-}cha} \approx 32.0\%$ at $w_2 = 10.6\%$. Wang et al. (2017) identified a value $f_{v\text{-}cha} \approx 28.4\%$ at $w_{opt\text{-}f} = 13.7\%$ under equivalent conditions. The increase of $f_{v\text{-}cha}$ with the decrease of water content could be explained by the swelling-shrinkage of fine soil. With the decrease of water content, the shrinkage of fine soil led to an increase of global volume of macro-pores. In that case, more coarse grains were required to constitute the global skeleton, giving rise to an increase of $f_{v\text{-}cha}$.

Comparison of $f_{v\text{-}cha}$ values obtained from monotonic and cyclic triaxial tests suggested that under a given water content, the value of $f_{v\text{-}cha}$ obtained under cyclic loading was slightly larger than that under monotonic loading, evidencing the more efficient effect of cyclic loading on the rearrangement of coarse grains.

ACKNOWLEDGEMENTS

This work was supported by the Chinese Scholar Council (CSC) and Ecole des Ponts ParisTech.

REFERENCES

ASTM D698-12. (2012). Standard test methods for laboratory compaction characteristics of soil using standard effort. ASTM International, West Conshohocken, Pa.

Cui, Y.J., Duong, T.V., Tang, A.M., Dupla, J.C., Calon, N. and Robinet, A., (2013). Investigation of the hydro-mechanical behaviour of fouled ballast. Journal of Zhejiang University Science A, 14(4), pp.244-255.

370 Cui, Y. J. (2018). Mechanical behaviour of coarse grains/fines mixture under monotonic and
371 cyclic loadings. Transportation Geotechnics, 17, 91-97.

372 Duong, T.V., Cui, Y.J., Tang, A.M., Dupla, J.C., Canou, J., Calon, N. and Robinet, A., (2016).
373 Effects of water and fines contents on the resilient modulus of the interlayer soil of
374 railway substructure. *Acta Geotechnica*, *11*(1), pp.51-59.

375 de Frias Lopez, R., Silfwerbrand, J., Jelagin, D., & Birgisson, B. (2016). Force transmission
376 and soil fabric of binary granular mixtures. Géotechnique, 66(7), 578-583.

377 Han, Z., & Vanapalli, S. K. (2015). Model for predicting resilient modulus of unsaturated
378 subgrade soil using soil-water characteristic curve. Canadian Geotechnical Journal,
379 52(10), 1605-1619.

380 Jibon, M., Mishra, D., & Kassem, E. (2020). Laboratory characterization of fine-grained soils
381 for Pavement ME Design implementation in Idaho. Transportation Geotechnics, 25,
382 100395.

383 Khasawneh, M. A., & Al-jamal, N. F. (2019). Modeling resilient modulus of fine-grained
384 materials using different statistical techniques. Transportation Geotechnics, 21, 100263.

385 Lin, S. Y., Lin, P. S., Luo, H. S., & Juang, C. H. (2000). Shear modulus and damping ratio
386 characteristics of gravelly deposits. Canadian Geotechnical Journal, 37(3), 638-651.

387 Lamas-lopez, F. (2016). Field and laboratory investigation on the dynamic behavior of
388 conventional railway track-bed materials in the context of traffic upgrade. PhD Thesis,
389 Ecole Nationale des Ponts et Chaussées, Université Paris-Est.

390 Menq, F. Y. (2003). Dynamic properties of sandy and gravelly soils. Ph.D. thesis, The
391 University of Texas at Austin.

392 Mousa, E., El-Badawy, S., & Azam, A. (2020). Evaluation of Reclaimed Asphalt Pavement as
393 Base/Subbase Material in Egypt. Transportation Geotechnics, 100414.

394 Ng, C. W. W., Zhou, C., Yuan, Q., & Xu, J. (2013). Resilient modulus of unsaturated
395 subgrade soil: experimental and theoretical investigations. Canadian Geotechnical Journal,
396 50(2), 223-232.

397 Qi, S., Cui, Y.J., Chen, R.P., Wang, H.L., Lamas-Lopez, F., Aimedieu, P., Dupla, J.C., Canou,
398 J. and Saussine, G., (2019). Influence of grain size distribution of inclusions on the
399 mechanical behaviours of track-bed materials. *Géotechnique*, pp.1-10.

400 Qi, S., Cui, Y. J., Dupla, J. C., Chen, R. P., Wang, H. L., Su, Y., ... & Canou, J. (2020).
401 Investigation of the parallel gradation method based on the response of track-bed
402 materials under cyclic loadings. Transportation Geotechnics, 100360.

403 Rollins, K. M., Evans, M. D., Diehl, N. B., & III, W. D. D. (1998). Shear modulus and
404 damping relationships for gravels. Journal of Geotechnical and Geoenvironmental
405 Engineering, 124(5), 396-405.

406 Stewart, H. E. (1982). The prediction of track performance under dynamic traffic loading.
407 Ph.D. thesis, University of Massachusetts.

408 Seed, H. B., Wong, R. T., Idriss, I. M., & Tokimatsu, K. (1986). Moduli and damping factors
409 for dynamic analyses of cohesionless soils. Journal of geotechnical engineering, 112(11),
410 1016-1032.

411 Selig, E. T., & Waters, J. M. (1994). Track geotechnology and substructure management.
412 Thomas Telford, London, U.K.

413 Seif El Dine, B., Dupla, J. C., Frank, R., Canou, J., & Kazan, Y. (2010). Mechanical
414 characterization of matrix coarse-grained soils with a large-sized triaxial device.
415 Canadian Geotechnical Journal, 47(4), 425-438.

416 Su, Y., Cui, Y.J., Dupla, J.C., Canou, J., Qi, S., (2020a). Developing a sample preparation
417 approach to study the mechanical behavior of unsaturated fine/coarse soil
418 mixture. *Geotechnical Testing Journal*. (In press)

419 Su, Y., Cui, Y. J., Dupla, J. C., & Canou, J. (2020b). Investigation of the effect of water
420 content on the mechanical behavior of track-bed materials under various coarse grain
421 contents. Construction and Building Materials, 263, 120206.

422 Tennakoon, N., & Indraratna, B. (2014). Behaviour of clay-fouled ballast under cyclic loading.
423 Géotechnique, 64(6), 502-506.

424 Trinh, V. N. (2011). Comportement hydromécanique des matériaux constitutifs de
425 plateformes ferroviaires anciennes. PhD Thesis, Ecole Nationale des Ponts et Chaussées,
426 Université Paris-Est.

427 Werkmeister, S., Dawson, A.R. and Wellner, F., (2004). Pavement design model for unbound
428 granular materials. Journal of Transportation Engineering, 130(5), pp.665-674.

429 Wang, H.L., Cui, Y.J., Lamas-Lopez, F., Dupla, J.C., Canou, J., Calon, N., Saussine, G.,
430 Aimedieu, P. and Chen, R.P., (2017). Effects of inclusion contents on resilient modulus
431 and damping ratio of unsaturated track-bed materials. *Canadian Geotechnical*
432 *Journal*, *54*(12), pp.1672-1681.

433 Wang, H.L., Cui, Y.J., Lamas-Lopez, F., Calon, N., Saussine, G., Dupla, J.C., Canou, J.,
434 Aimedieu, P. and Chen, R.P., (2018a). Investigation on the mechanical behavior of track-
435 bed materials at various contents of coarse grains. *Construction and Building*
436 *Materials*, *164*, pp.228-237.

437 Wang, H.L., Cui, Y.J., Lamas-Lopez, F., Dupla, J.C., Canou, J., Calon, N., Saussine, G.,
438 Aimedieu, P. and Chen, R.P., (2018b). Permanent deformation of track-bed materials at
439 various inclusion contents under large number of loading cycles. *Journal of Geotechnical*
440 *and Geoenvironmental Engineering*, *144*(8), p.04018044.

441 Yang, S. R., Lin, H. D., Kung, J. H., & Huang, W. H. (2008). Suction-controlled laboratory
442 test on resilient modulus of unsaturated compacted subgrade soils. Journal of
443 Geotechnical and Geoenvironmental Engineering, 134(9), 1375-1384.

444 Zhang, L.M. and Li, X., (2010). Microporosity structure of coarse granular soils. *Journal of*
445 *Geotechnical and Geoenvironmental Engineering*, *136*(10), pp.1425-1436.

446 Zhalehjoo, N., Tolooiyan, A., Mackay, R., & Bodin, D. (2018). The effect of instrumentation
447 on the determination of the resilient modulus of unbound granular materials using
448 advanced repeated load triaxial testing. Transportation Geotechnics, 14, 190-201.

449

450 NOTATION

D_r	damping ratio
ε_1	axial strain
$\Delta\varepsilon_1$	increase of axial strain
ε_1^r	resilient strain
ε_1^p	permanent strain
ε_v^p	plastic volumetric strain
ε_v	volumetric strain
E_{loop}	area of hysteresis loop
E_d	area of triangle
f_v	volumetric coarse grain content
$f_{v\text{-}cha}$	characteristic volumetric coarse grain content
M_r	resilient modulus
N	number of loading cycles
ρ_d	dry density of sample
$\rho_{dmax\text{-}f}$	maximum dry density of fine soil
q	deviator stress
q_{max}	maximum deviator stress
q_{min}	minimum deviator stress

Δq	deviator stress amplitude
S_r	degree of saturation
$w_{\text{opt-f}}$	optimum water content of fine soil
w_{f}	water content of fine soil
σ_3	confining pressure

451

452 LIST OF TABLES

453

LIST OF FIGURES

454

Table 1. Nine different commercial soils used for fine soil preparation

Soil classification	Commercial Soil	Mass proportion (%)	The range of grain size (mm)
Sand	HN34	3.3	0.063 - 0.50
	HN31	3.3	0.16 - 0.63
	HN0.4-0.8	6.7	0.25 - 1
	HN0.6-1.6	6.7	0.32 - 2
	HN1-2.5	13.3	0.32 – 3.20
Clay	C4	16.7	0.0009 – 0.50
	C10	20	0.0009 – 0.25
	Speswhite	23.3	0.0003 – 0.01
	Bentonite	6.7	0.001 – 0.01

Table 2. Experimental program

f_v (%)	Initial water content $w_{opt\text{-}f}$ (%)	Target w_f (%)	Target S_r (%)	Target $\rho_{dmax\text{-}f}$ (Mg/m^3)	Target ρ_d (Mg/m^3)	Measured ρ_d (Mg/m^3)
0	13.7	17.6	100	1.82	1.82	1.80
		10.6	60			1.85
10		17.6	100		1.91	1.88
		10.6	60			1.93
20		17.6	100		1.99	1.97
		10.6	60			2.01
35		17.6	100		2.12	2.11
		10.6	60			2.13
45		17.6	100		2.21	2.20
		10.6	60			2.22

Note: f_v represents the volumetric ratio of dry coarse grains to the total sample. $w_{opt\text{-}f}$, w_f, S_r and $\rho_{dmax\text{-}f}$ represent the optimum water content, the water content, the degree of saturation and the maximum dry density of fine soils, respectively. ρ_d represents the dry density of soil mixtures sample. Measured ρ_d represents the dry density of soil mixtures sample after wetting or drying from compaction water content $w_{opt\text{-}f}$ to target w_f.

Table 3. Variation of $f_{v\text{-}cha}$ with water content

w (%)	17.6	13.7	10.6
$f_{v\text{-}cha}$ (%)	25.5	28.4	32.0

Note: $f_{v\text{-}cha} \approx 28.4\%$ at $w_{opt\text{-}f} = 13.7\%$ was obtained by Wang et al. (2017)

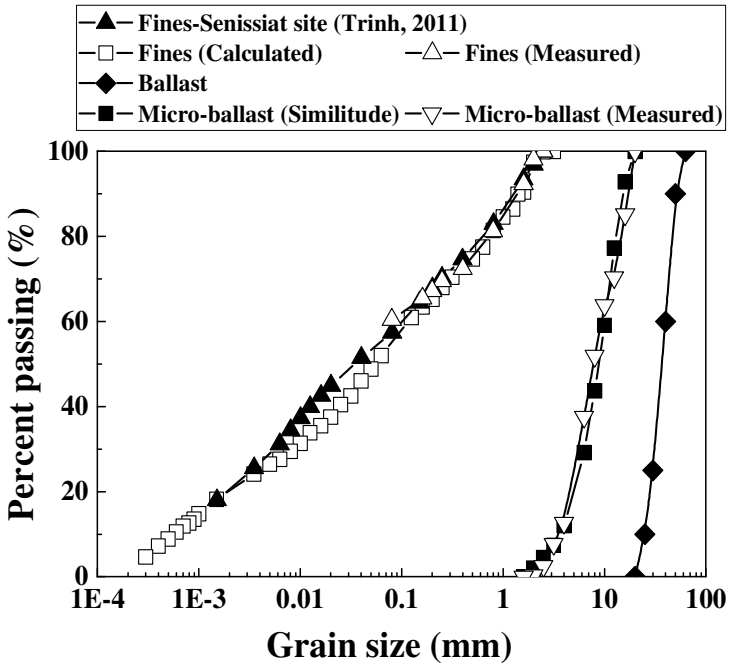

496

497 Fig. 1. Grain size distribution curves of fines and micro-ballast (after Wang et al. 2018a)

498

499

500

501

502

503

504

505

506

507

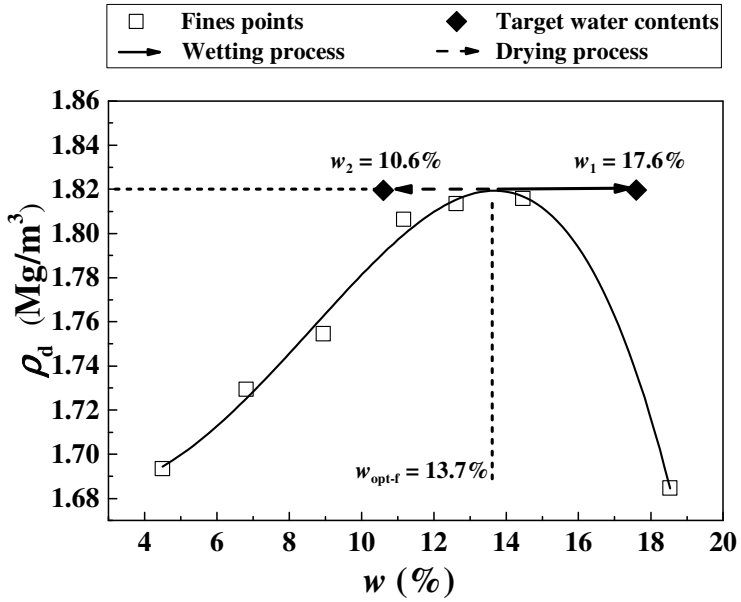

Fig. 2. Samples states at two target water contents with respect to the compaction curve

508

509

510

511

512

513

514

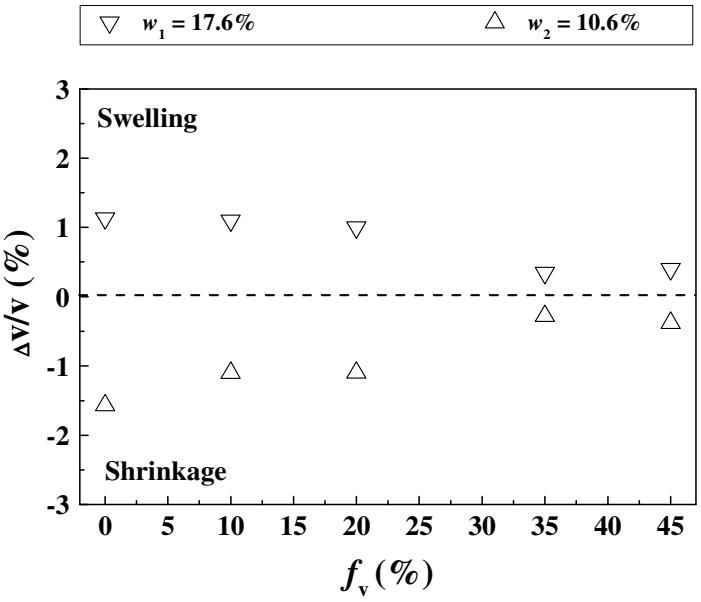

Fig. 3. Volume change of samples with f_v at two target water contents

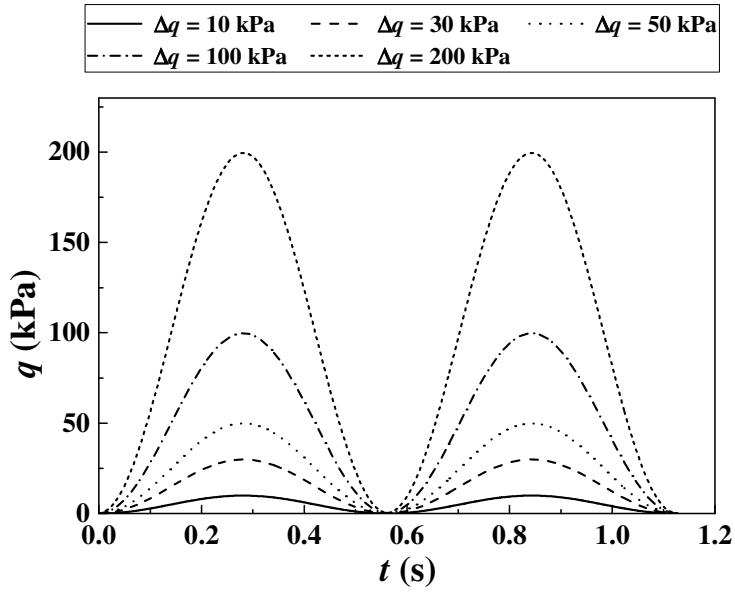

523

524 Fig. 4. Typical sine-shaped signals with various stress amplitudes Δq

525

526

527

528

529

530

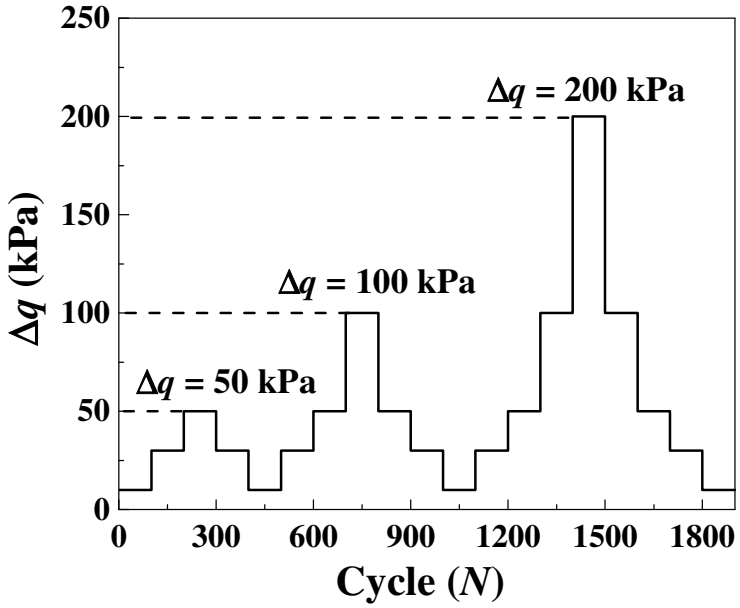

Fig. 5. Multi-step loading procedure applied in cyclic triaxial tests

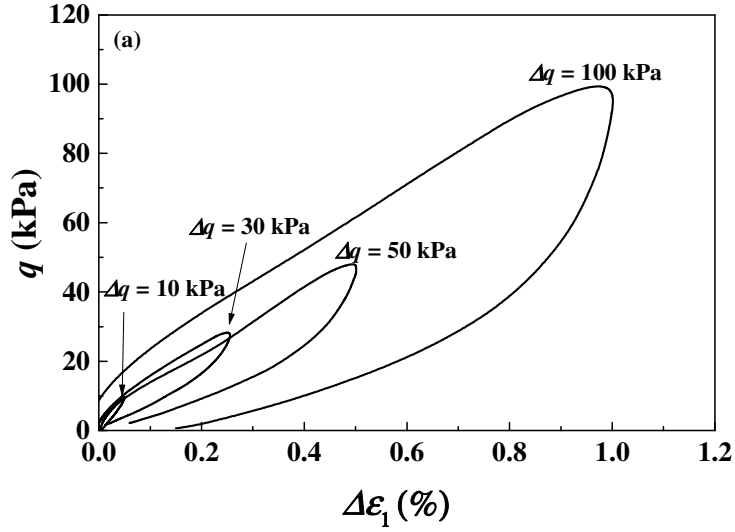

539

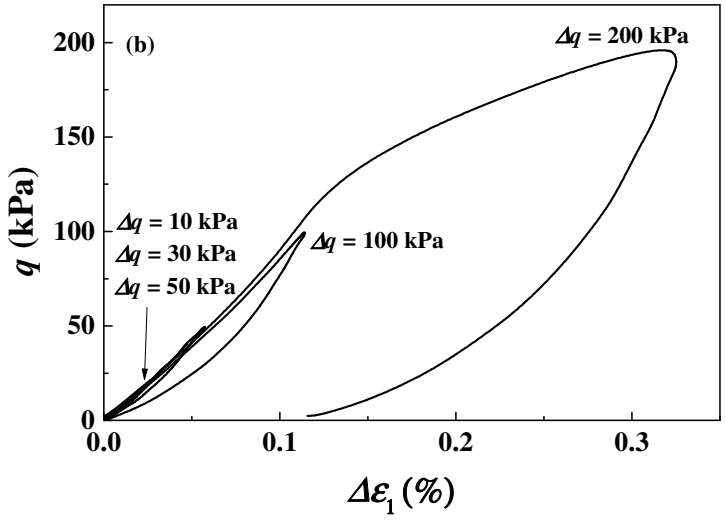

540

541 Fig. 6. Typical hysteresis loops for various deviator stress amplitudes Δq at $f_v = 0\%$ and two
542 target water contents: (a) $w_1 = 17.6\%$; (b) $w_2 = 10.6\%$

543

544

545

546

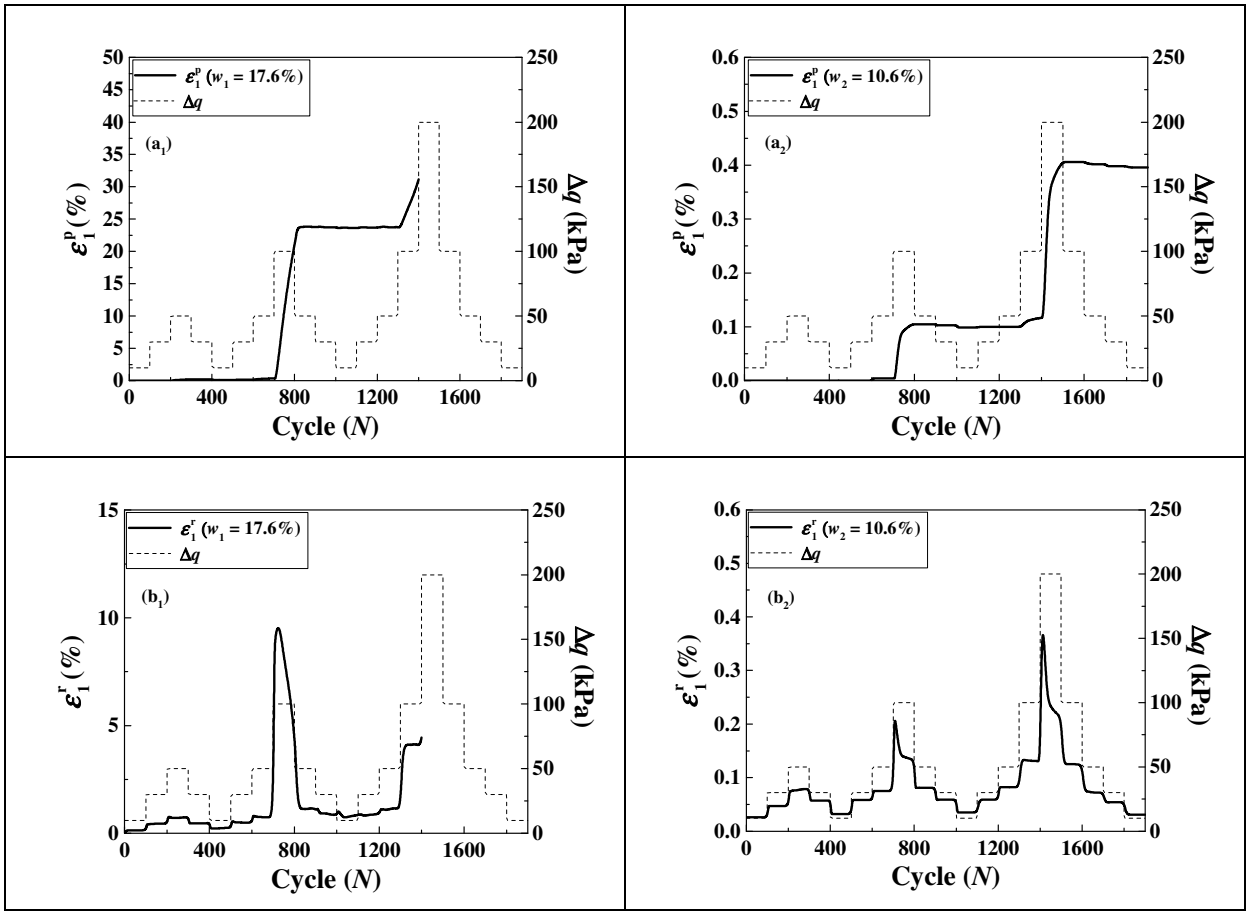

Fig. 7. Variations of permanent strain and resilient strain with loading cycles at f_v = 0% and two target water contents: (a$_1$) - (b$_1$) w_1 = 17.6%; (a$_2$) - (b$_2$) w_2 = 10.6%

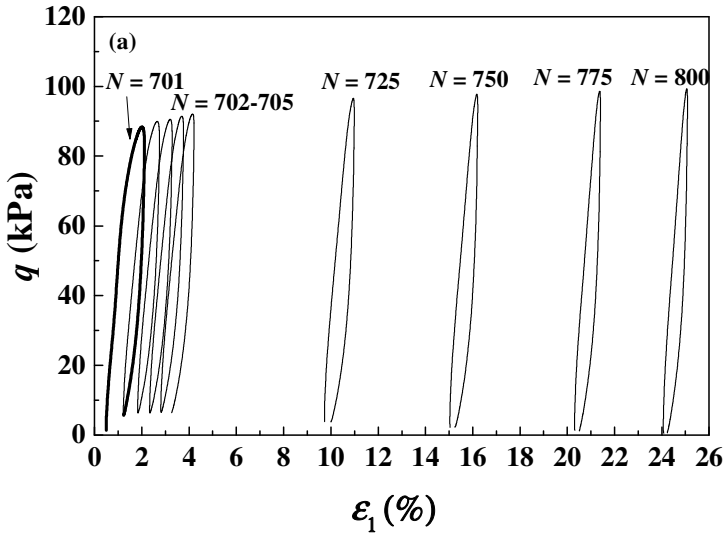

555

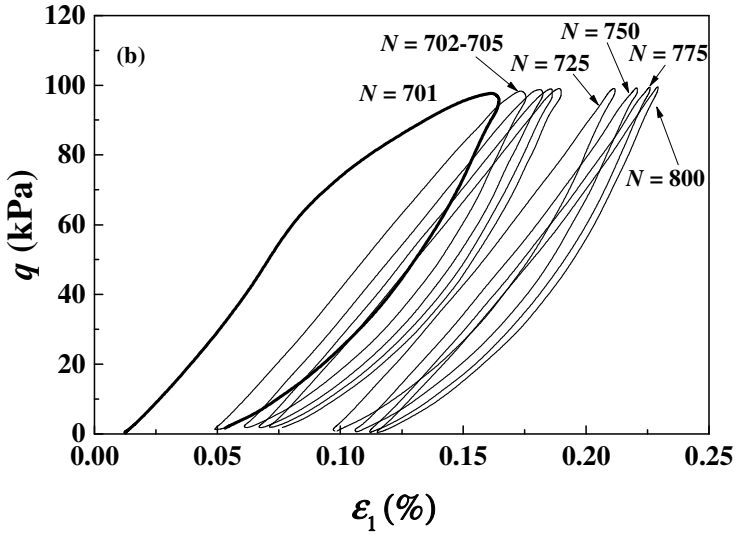

556

557 Fig. 8. Hysteresis loops at the first 100 loading cycles (N = 701- 800) of Δq = 100 kPa for the
558 samples at f_v = 0% and two target water contents: (a) w_1 = 17.6%; (b) w_2 = 10.6%

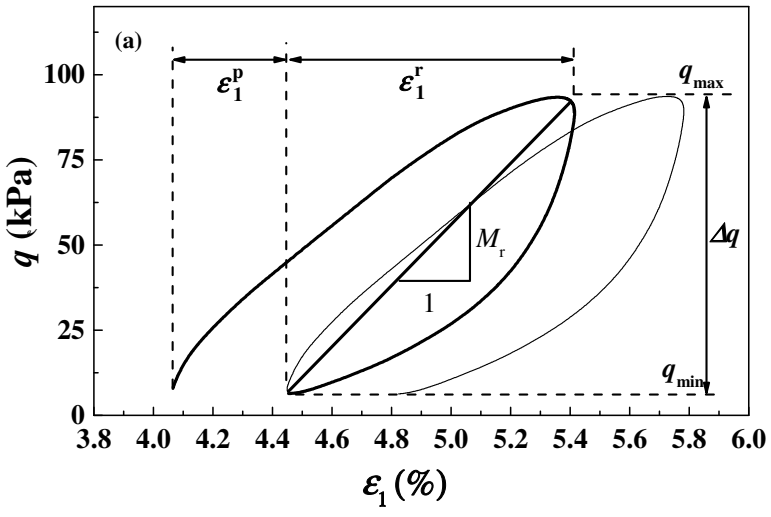

559

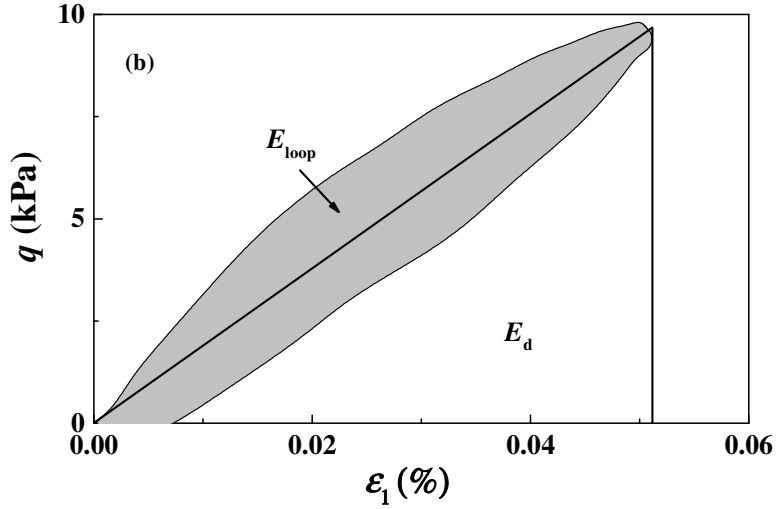

560

561 Fig. 9. Determination of (a) resilient modulus M_r and (b) damping ratio D_r

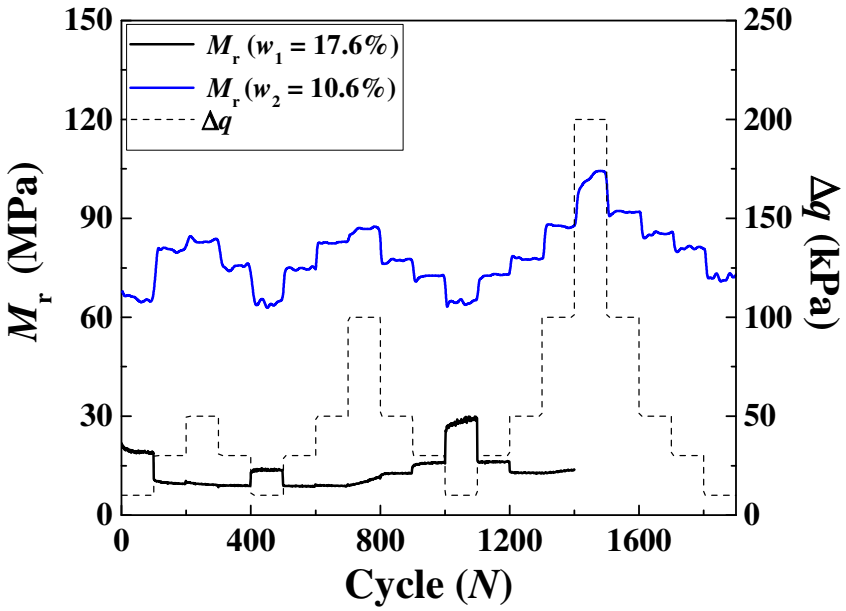

562

563 Fig. 10. Variations of M_r with number of loading cycles N at f_v = 0% and two target water
564 contents

565

566

567

568

569

570

571

572

573

574

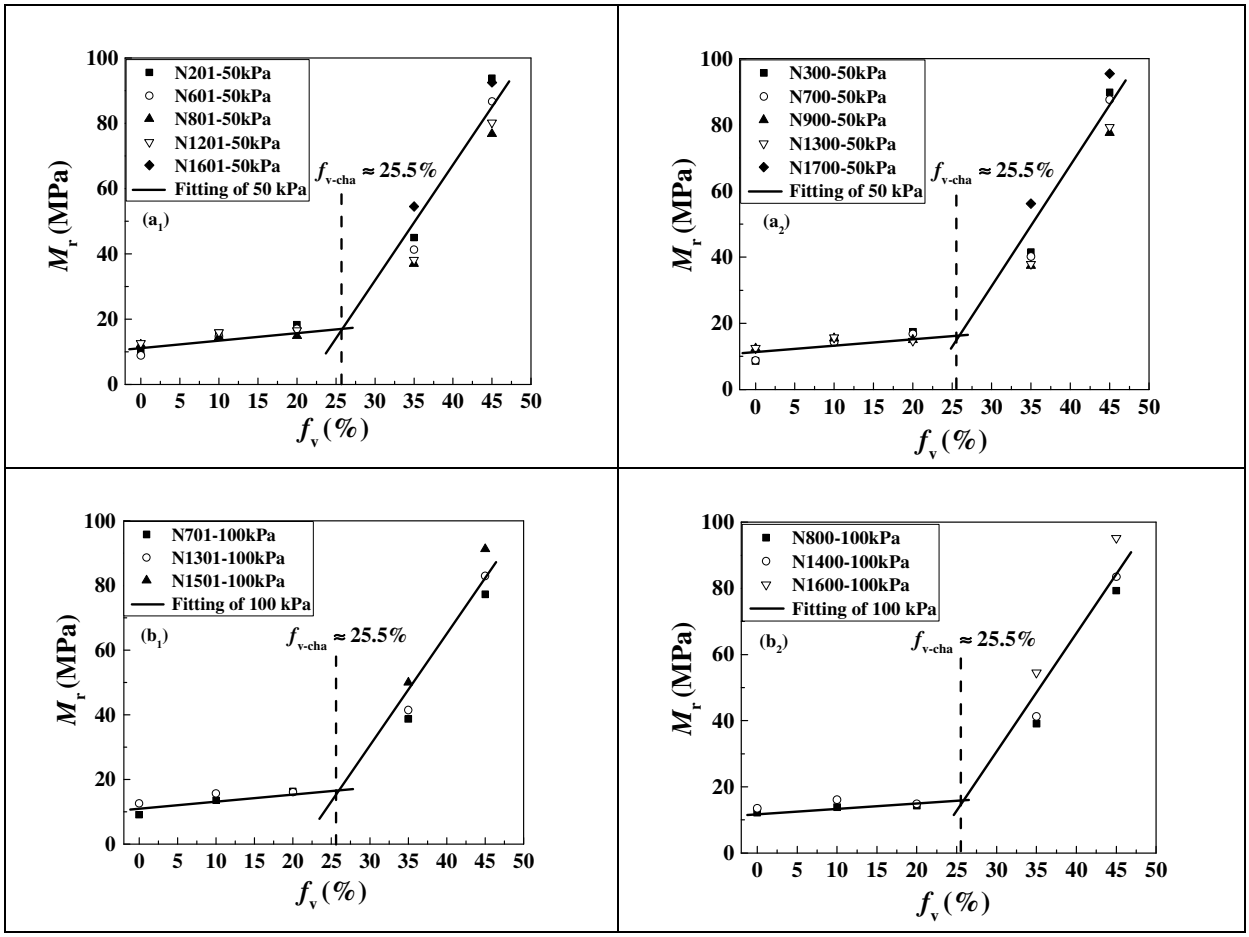

Fig. 11. Variations of M_r with f_v at w_1 = 17.6% and (a_1) start-stage of Δq = 50 kPa, (b_1) start-stage of Δq = 100 kPa, (a_2) end-stage of Δq = 50 kPa and (b_2) end-stage of Δq = 100 kPa

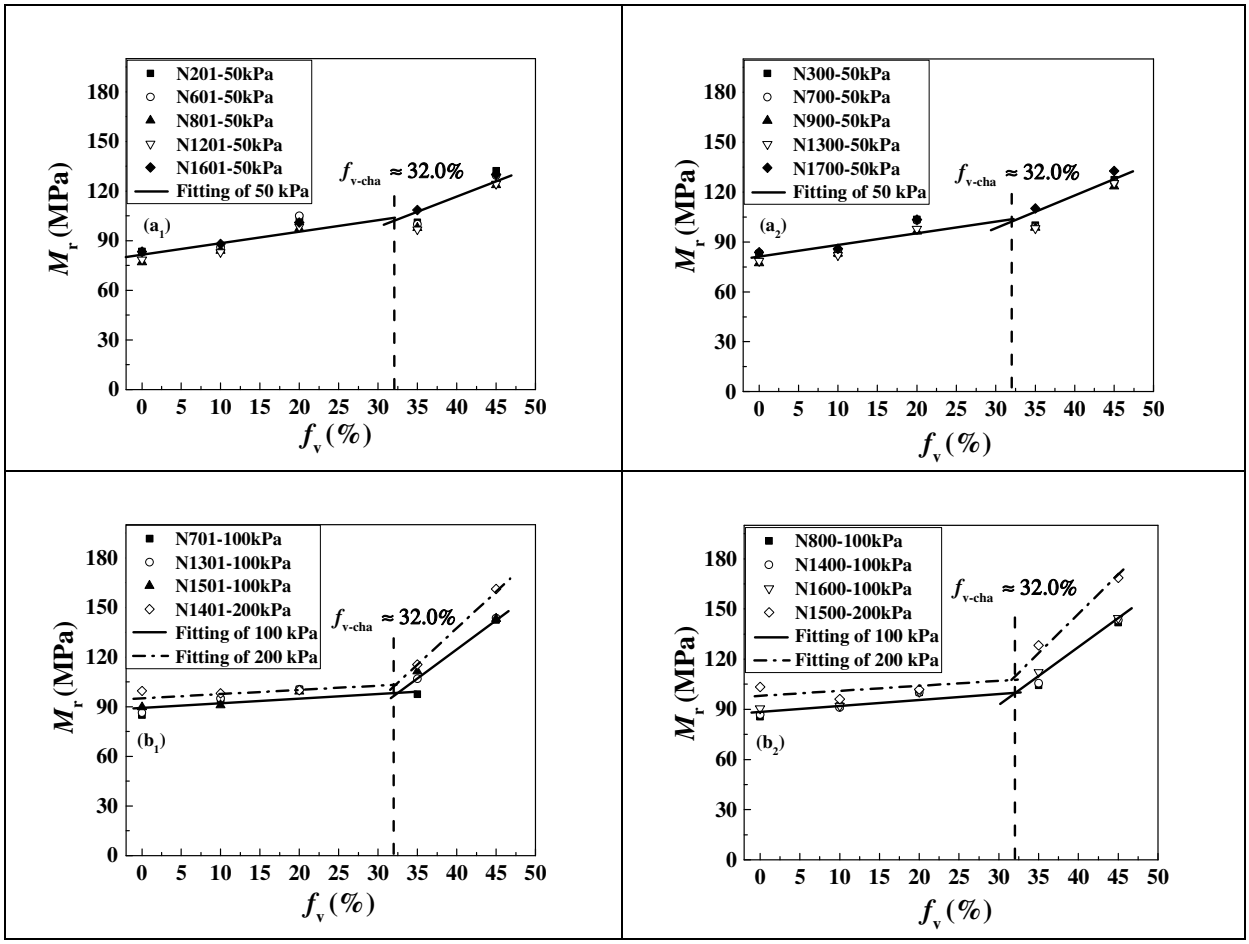

589

590 Fig. 12. Variations of M_r with f_v at w_2 = 10.6% and (a_1) start-stage of Δq = 50 kPa, (b_1) start-
591 stage of Δq = 100 and 200 kPa, (a_2) end-stage of Δq = 50 kPa and (b_2) end-stage of Δq = 100
592 and 200 kPa

593

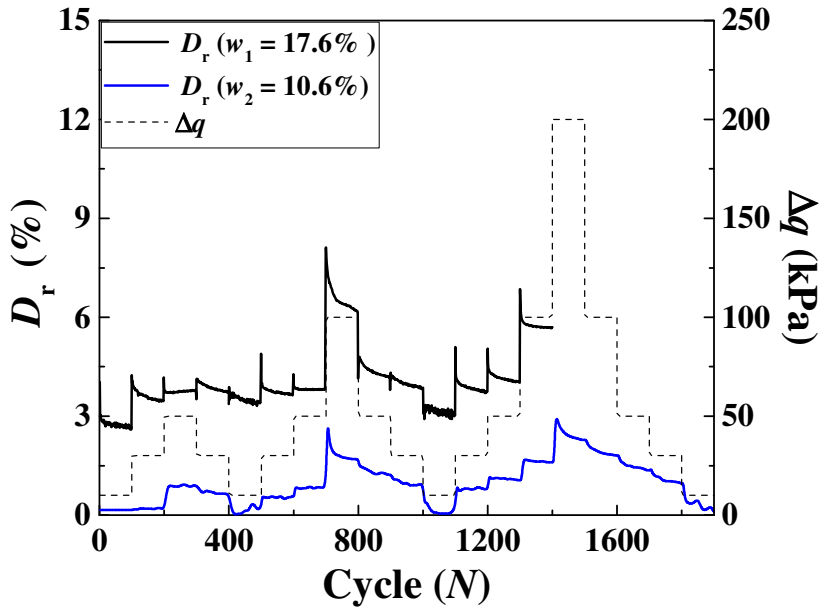

Fig. 13. Variations of D_r with loading cycles N at f_v = 0% and two target water contents

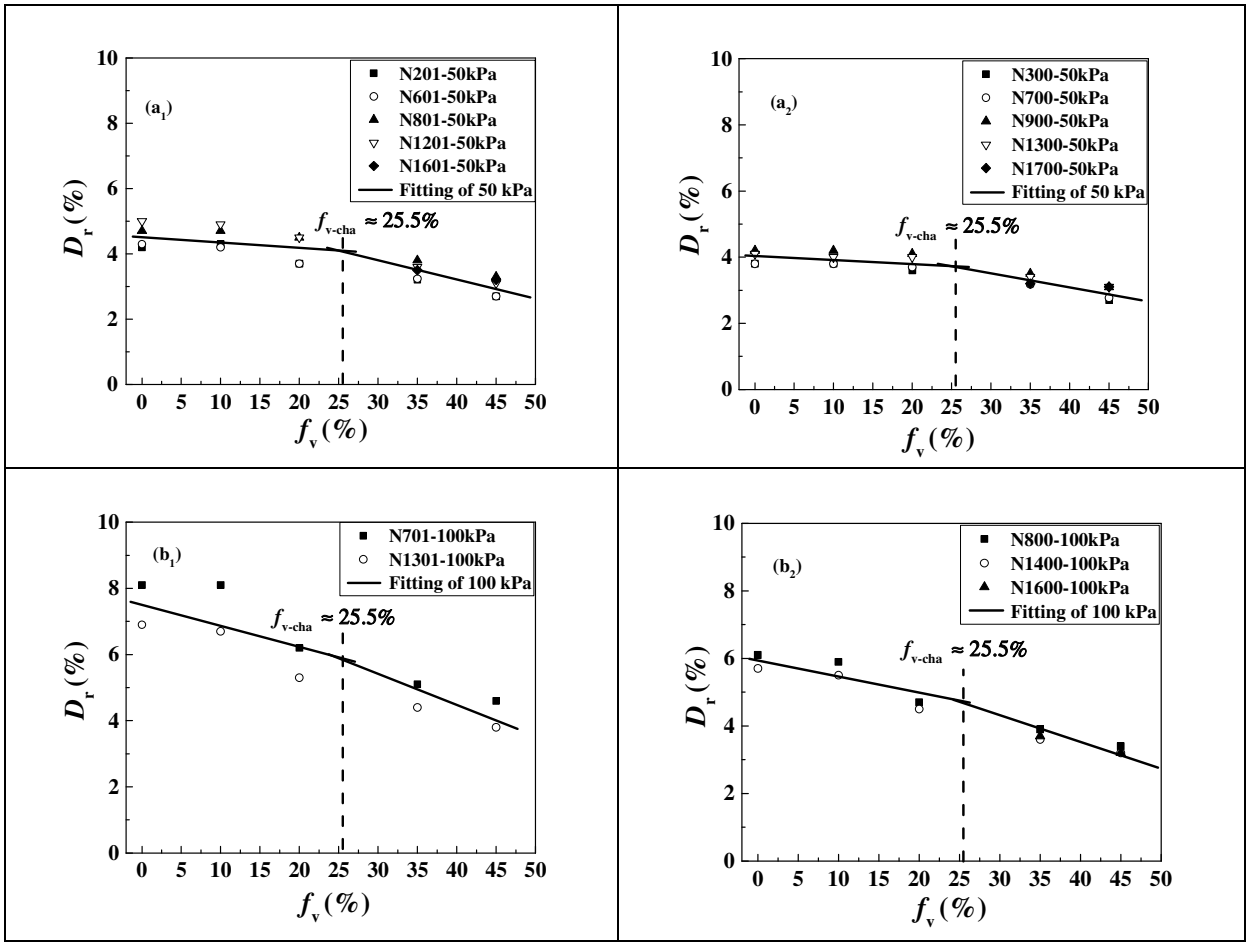

606

607 Fig. 14. Variations of D_r with f_v at w_1 = 17.6% and (a_1) start-stage of Δq = 50 kPa, (b_1) start-
608 stage of Δq = 100 kPa, (a_2) end-stage of Δq = 50 kPa and (b_2) end-stage of Δq = 100 kPa

609

610

611

612

613

614

615

616

617

618

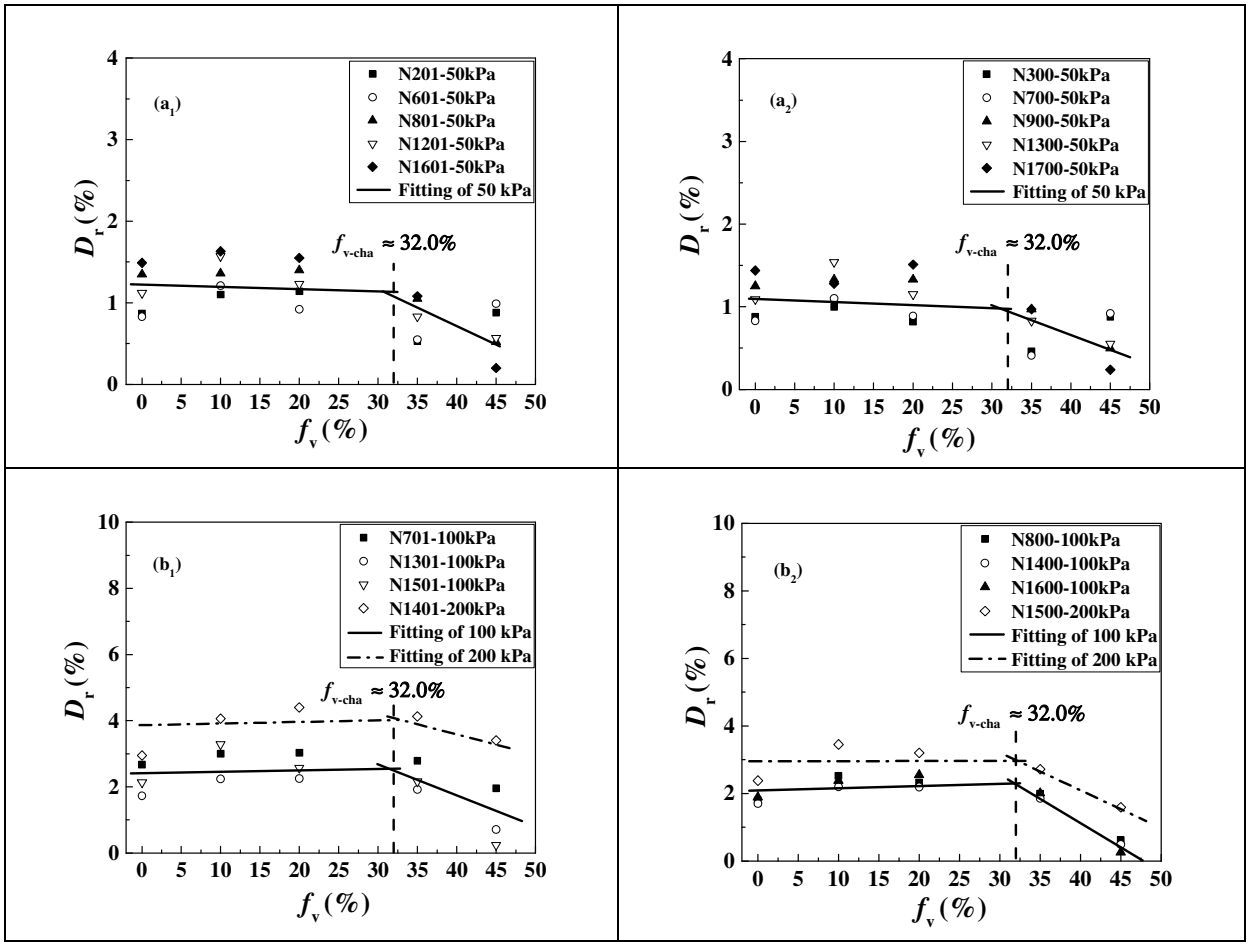

Fig. 15. Variations of D_r with f_v at w_2 = 10.6% and (a_1) start-stage of Δq = 50 kPa, (b_1) start-stage of Δq = 100 and 200 kPa, (a_2) end-stage of Δq = 50 kPa and (b_2) end-stage of Δq = 100 and 200 kPa